

YONGWOOK SONG¹, DAEYOUNG KIM¹, SEUNGJIN NAM¹,
KEE-AHN LEE², HYUNJOO CHOI^{1*}

EFFECT OF MILLING DURATION ON OXIDE-FORMATION BEHAVIOR OF OXIDE-DISPERSION-STRENGTHENED HIGH-ENTROPY ALLOYS

Oxide-dispersion-strengthened high-entropy alloys were produced by hot-pressing a ball-milled mixture of Y_2O_3 and atomized CoCrFeMnNi powder. The effect of milling duration on grain size reduction, oxide formation behavior, and the resulting mechanical properties of the alloys was studied. Both the alloy powder size and Y_2O_3 particle size decreased with milling time. Moreover, the alloy powder experienced severe plastic deformation, dramatically generating crystalline defects. As a result, the grain size was reduced to ~ 16.746 nm and in-situ second phases (e.g., MnO_2 and σ phase) were formed at the defects. This increased the hardness of the alloys up to a certain level, although excessive amounts of in-situ second phases had the reverse effect.

Keywords: Oxide dispersion strengthening, High entropy alloys, Severe plastic deformation, In situ second phases, Milling time effects

1. Introduction

The equiatomic CoCrFeMnNi high-entropy alloy (HEA) is a representative face-centered cubic (FCC) HEA, which is the earliest HEAs developed by Cantor [1] and has been extensively studied because of its good strength and ductility at cryogenic temperatures [2,3]. However, its commercial use has been limited by its relatively low yield strength at room temperature [4]. Efforts have been made to increase its strength by refining the grain size into the ultrafine- [5-8] or nano-regime [9,10] using severe plastic deformation (SPD) techniques. However, very limited study was reported on enhancing strength of HEAs by dispersing hard phases such as nano-scale ceramic phases.

Oxide-dispersion-strengthened (ODS) metals have attracted a great deal of attention because of their unique structural feature: small oxide particles uniformly dispersed at a very high number density ($\sim 10^{24} \text{ m}^{-3}$) [11-13]. These nanoscale particles prevent the motion of dislocations and provide a high density of pinning sites for grain boundaries, thereby increasing the flow stress of the metallic matrix and stabilizing the high-temperature microstructure. Hence, in or ex situ dispersion of nano-sized particles should be considered as a strategy to increase the yield strength of Cantor HEAs.

The standard process for creating an ODS alloy consists of ball-milling Y_2O_3 and pre-alloyed powders, then consolidating the milled powder by thermo-mechanical processes [14,15]. Optimizing this requires investigating the formation and subsequent evolution of the nanoscale oxide particles. In general, Y_2O_3 particles have been reported to be dissolved into the metallic matrix during ball milling and then to form nanoscale oxides during subsequent thermomechanical processes. For ODS-HEA alloys, however, oxide formation behavior is little studied.

This work focuses on the oxide-formation mechanism of ODS-HEA alloys. We investigate the microstructural evolution of ODS-HEA alloys with various milling durations. The objective is to identify the evolution mechanism and determine the influence of milling time on the characteristics of nanoscale oxides.

2. Experimental

The ODS CoCrFeMnNi HEA matrix composites were manufactured via powder metallurgy. CoCrFeMnNi HEA powders ($< 150 \mu\text{m}$) were prepared by atomization. Subsequently, 3 wt.% of Y_2O_3 nanoparticles (50-80 nm) were dispersed within the powders through high-energy ball milling using an attrition

¹ KOOKMIN UNIVERSITY, SCHOOL OF MATERIALS SCIENCE AND ENGINEERING, SEOUL, REPUBLIC OF KOREA;

² INHA UNIVERSITY, DEPARTMENT OF MATERIALS SCIENCE AND ENGINEERING, INCHEON 22212, REPUBLIC OF KOREA

* Corresponding author: hyunjoo@kookmin.ac.kr



mill (KMC-2BV, KMC Co. Ltd.) with stainless steel balls (1000 g; diameter: 5 mm) as a milling medium and 3 g of stearic acid ($\text{CH}_3(\text{CH}_2)_{16}\text{CO}_2\text{H}$, Sigma Aldrich Korea Co, Ltd). Milling was conducted at 500 rpm for various times (12, 24, and 48 h) under an Ar atmosphere. The as-milled powders were compacted in a stainless-steel mold with boron nitride as a lubricant. Subsequently, hot pressing was conducted at 600°C for 2 h under a uniaxial pressure of ~70 MPa.

The morphology and size of the starting materials (HEA powders and Y_2O_3 nanoparticles) and the as-milled composite powders were observed using scanning electron microscopy (SEM, JEOL JSM 2001F). The phase and crystal structures were analyzed using an XPD (Rigaku Ultima iii X-ray diffractometer and SmartLab) with a Cu K α radiation source. The starting materials, the as-milled composite powders, and the as-pressed composites were examined in a 2θ scan range from 20° to 110° with a scanning speed of 10°/min. The type of oxide in the as-pressed composites was investigated by XPS (Thermo, K-alpha). The microstructure of the as-prepared composites and the dispersion of the Y_2O_3 particles were observed using optical microscopy (OM), an SEM equipped with an EDS probe, and a high-resolution transmission electron microscope (HR-TEM, JEOL JEM-2100F) equipped with an EDS. The grain size of the composites was calculated based on HR-TEM bright-field images obtained via an image analyzer (ImageJ software version 1.52a). The line intercept method was implemented five times in different areas in each image to enhance the reliability. The room-temperature hardness of the composites was measured using a micro-Vickers hardness tester (Mitutoyo, HM-211) with a load of 0.5 kg and duration of 10 s. The surface of the composites was polished before the hardness test.

3. Results and discussion

Fig. 1 shows SEM images of the starting CoCrFeMnNi (Fig. 1(a)), nano-sized Y_2O_3 particles (Fig. 1(b)), and as-milled ODS CoCrFeMnNi matrix composite powders with various milling times. Before milling, the CoCrFeMnNi HEA particles showed a spherical morphology, while the Y_2O_3 particles agglomerated because of their small size and large specific surface area. The powder experienced severe plastic deformation, and the powder morphology changed from spherical to flattened [16]. Furthermore, the particle size of the composites decreased because of repeated shattering and fracturing [17,18].

Fig. 2 shows the XRD patterns of the starting materials (HEA powders and Y_2O_3 particles), as-milled composite powders with various milling times (12, 24, and 48 h) (Fig. 2(a)), and as-pressed ODS composites (Fig. 2(b)). After milling, the composite powders have FCC and Y_2O_3 peaks, regardless of the milling time. Despite the high milling energy and consolidation temperature, the FCC phase of the HEA matrix and Y_2O_3 maintained their phases without any chemical reaction through the whole process. However, Mn oxide and σ phase appeared within the composites after milling for 24 and 48 h, as shown in Figure 2(c). Mn oxide formed by the reaction between the CoCrFeMnNi HEA matrix and the air: Mn has a high oxygen affinity. The σ phase was formed during the hot-pressing process because of its phase stability within the HEA matrix region at temperatures ranging from 600 to 800°C [19,20]. Moreover, the intensity of the peaks corresponding to Mn oxide and σ phase increased with milling time. Dislocations, which are copiously generated during mechanical milling, may act as heterogeneous nucleation sites for new phases in the composites. Therefore, the composite milled for 48 h had

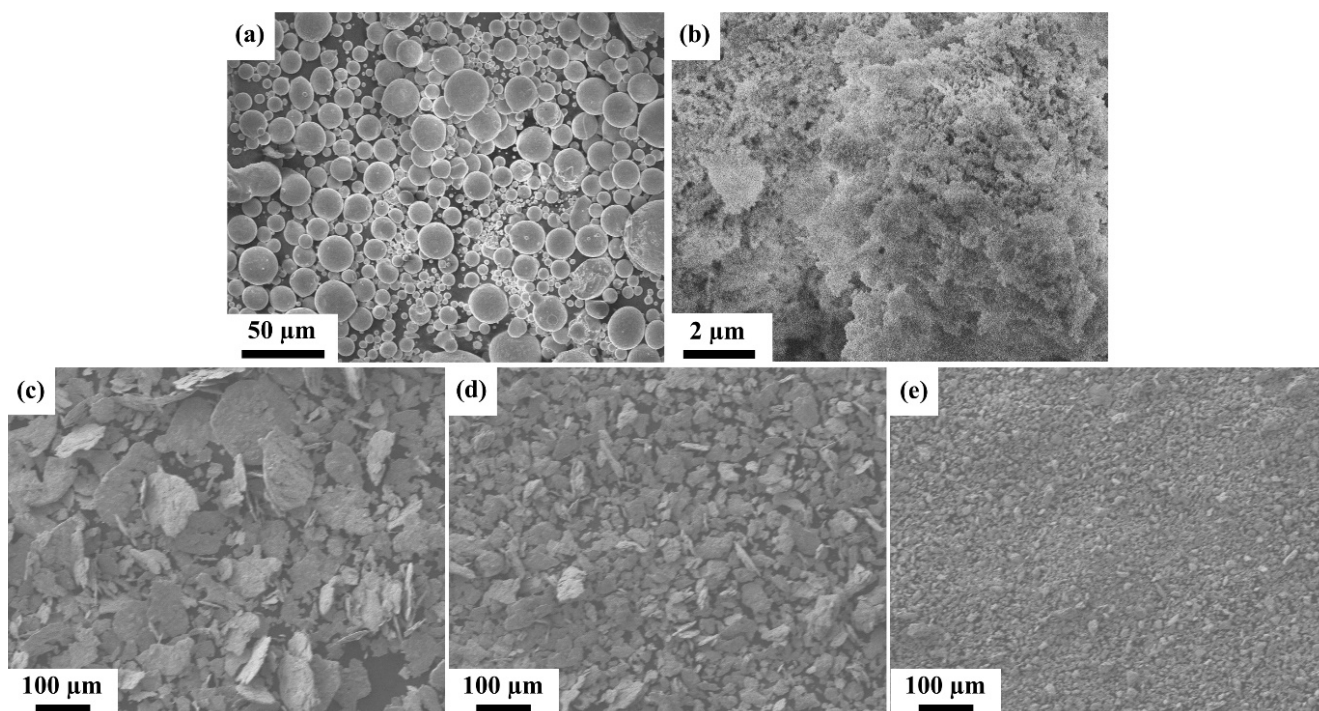


Fig. 1. Scanning-electron-microscope images of (a) starting high-entropy-alloy particles; (b) Y_2O_3 nano-sized particles; and (c)-(e) composite powders after milling for (c) 12 h; (d) 24 h; and (e) 48 h

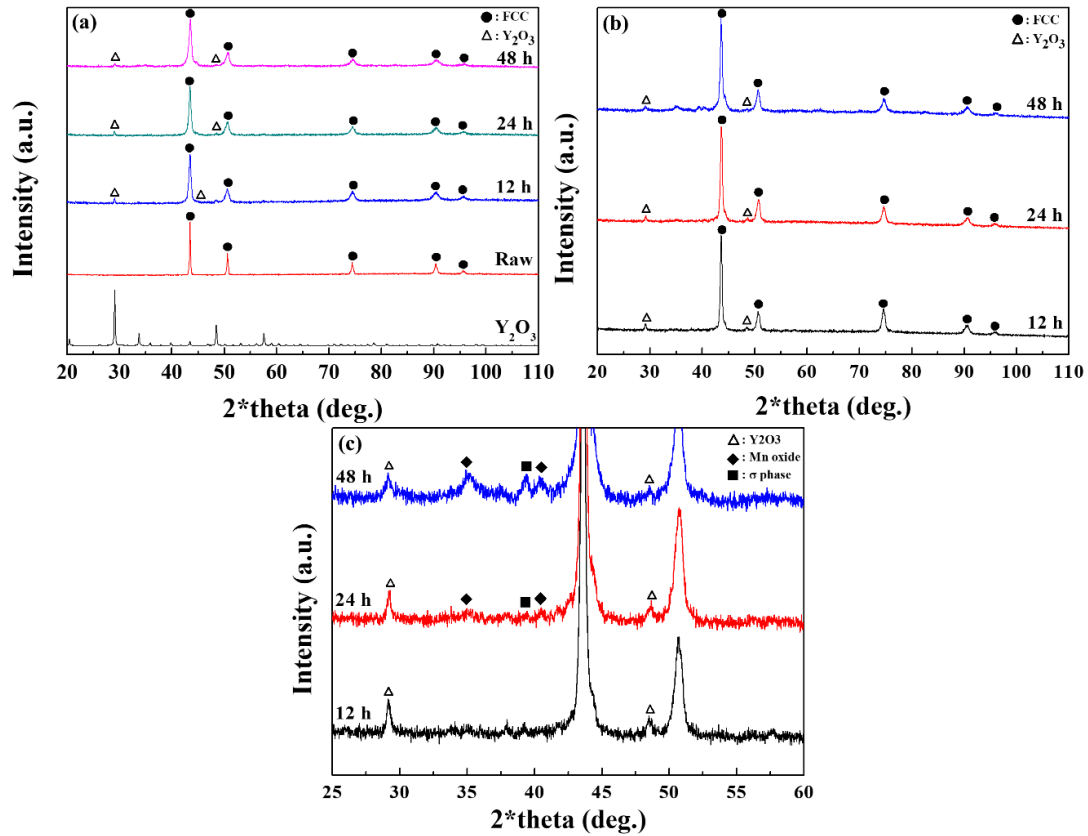


Fig. 2. X-ray diffraction spectra of (a) the starting materials (HEA particles and Y_2O_3 nano-particles) and the composite powders after milling for various times (12, 24, and 48 h); and (b) the as-pressed composites. (c) An enlarged detail of (b) for the range 25° to 60° . Peaks corresponding to the FCC, Y_2O_3 , Mn oxide, and σ phases are marked

the highest number of nucleation sites and highest intensity of Mn oxide and σ phase. The peak corresponding to Y_2O_3 particles broadened with increasing milling times, possibly because of the reduction in the size of the Y_2O_3 particles with milling.

XPS analysis was conducted to identify the type of oxides of Mn in each composite. Figure 3 shows the XPS Mn2p spectra of the as-pressed composites. Only MnO_2 phases were detected

in the composites produced using 48-h-milled powder, while the 12- and 24-h-milled composites also exhibited MnO as well as MnO_2 phases. As is observable in Fig. 1, the HEA powder was gradually refined by milling; therefore, the longer-milled powder had a higher specific surface area and larger amount of surface oxides. Mn had more opportunity to react with oxygen during hot-pressing because more oxygen was supplied from

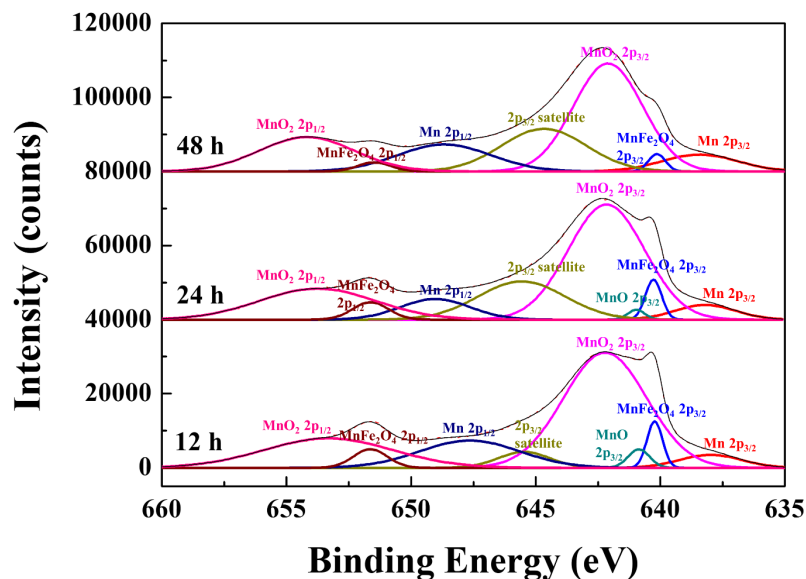


Fig. 3. Mn2p X-ray photoelectron spectra of the as-pressed composites for various milling times (12, 24, and 48 h)

the powder surface. Hence, stable MnO_2 could be more easily formed in the 48-h-milled composites.

Supplementary Figs. 1 and 2 are OM and SEM images, respectively, of the as-pressed composites, which had a high pore fraction on their surface. Thus, the composites were not completely consolidated by the hot-pressing process. However, the pore size of the composites decreased, and the number of particle boundaries increased, with increasing milling time. Moreover, the dispersion of the Y_2O_3 nanoparticles was more homogenized with long milling times, as shown in the SEM-EDS maps of the as-pressed ODS composites (Supplementary Fig. 3). Formation of Mn oxides in the composites was also observed in the EDS maps.

In TEM images and EDS maps of the ODS composites (Fig. 4), large and small HEA powders appeared to form a laminate structure wherein small Y_2O_3 particles were mainly detected in the small HEA powder, while Mn oxides were observed throughout the composites. Although oxide particles and metallic

matrix do exhibit coherency and a tight interface because of the significant differences in their lattice parameters and low wetting ability, the coherency and interface bonding can be considered satisfactory under the given condition because of the small sizes of the in situ formed oxide particles [21]. On the other hand, the average grain sizes of the as-pressed ODS composites using powders milled for 12, 24, and 48 h were 23.93 ± 4.02 , 20.29 ± 2.29 , and 16.75 ± 2.16 nm, respectively. The grain size of the composite was reduced by milling because of dynamic recrystallization and did not grow significantly during hot-pressing [22,23].

Figure 5 shows the average grain size and Vickers hardness of the as-pressed ODS composites with various milling times. The Vickers hardness of the as-pressed composites using powder milled for 12, 24, or 48 h was 250.0 ± 30.31 , 349.6 ± 16.73 , or 336.1 ± 12.04 HV, respectively. As previously mentioned, the average grain size of the composites decreased with an increase in the milling time owing to the high milling energy. Thus, the

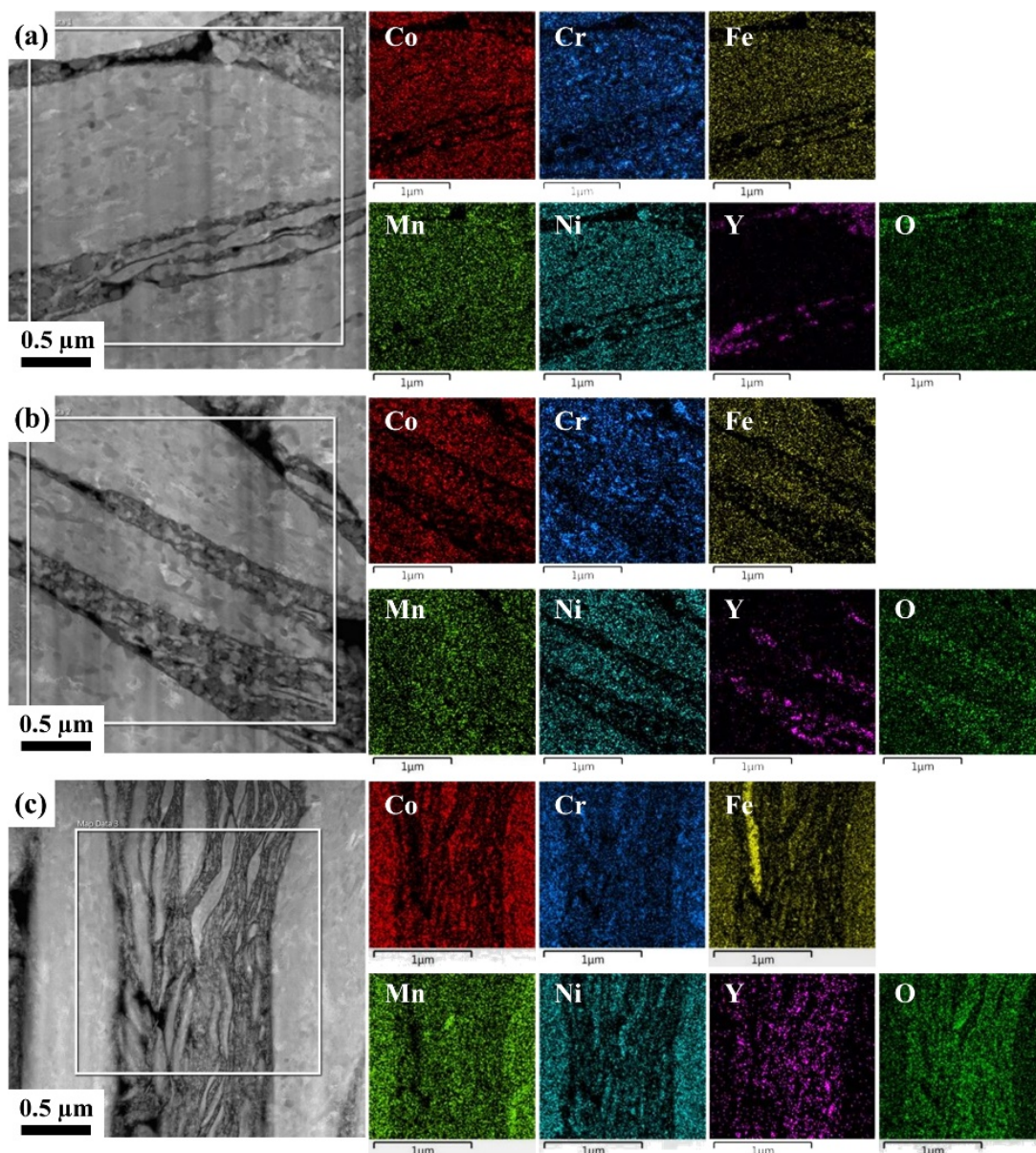
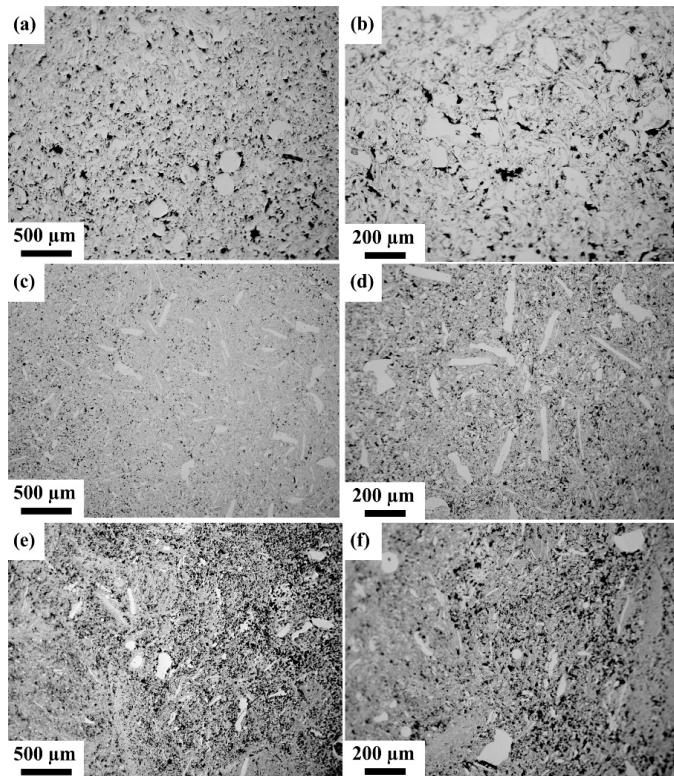


Fig. 4. High-resolution transmission-electron-microscope bright-field images and energy-dispersive spectroscopic maps of the as-pressed composites for various milling times: (a, b) 12 h, (c, d) 24 h, and (e, f) 48 h

hardness of the ODS composites milled for 24 and 48 h was higher than that of the composite using powder milled for 12 h because the effect of grain-boundary strengthening increased with milling time.

The size and dispersion of the Y_2O_3 nanoparticles also influence the mechanical properties of the composites. As observed in Figure 2(c), the Y_2O_3 particle size decreased with milling and the effect of dispersion strengthening improved with increasing milling time. Although the milling times were higher, the hardness of the composite milled for 48 h was smaller than that of the composite milled for 24 h. This is due to the in-situ second phases (e.g., Mn oxides and σ phase) that occur within the composite during the hot-pressing process, and that commonly show higher strength and lower ductility than the matrix. Nevertheless, MnO_2 is brittle compared to MnO. We found that, unlike the other composites, the 48-h-milled powder contained primarily MnO_2 ; consequently, its hardness was reduced, the brittleness of the oxide offsetting the reinforcing effect. This shows that different milling times will result in different types of oxides with different properties, and therefore that an optimal milling time must exist. The composite milled for 24 h had the correct fraction of the in-situ phase due to the optimal milling-process condition. On the other hand, the composite using powder milled for 12 h did not have enough in-situ second phase (and thus had the lowest hardness), whereas the composite milled for 48 h had too much (and thus also experienced reduced hardness). The composite with a milling time of 24 h had the highest hardness because it had the optimal milling conditions.



Supplementary Fig. 1. Optical-microscope images of the as-pressed composites for various milling times: (a, b) 12 h, (c, d) 24 h, and (e, f) 48 h

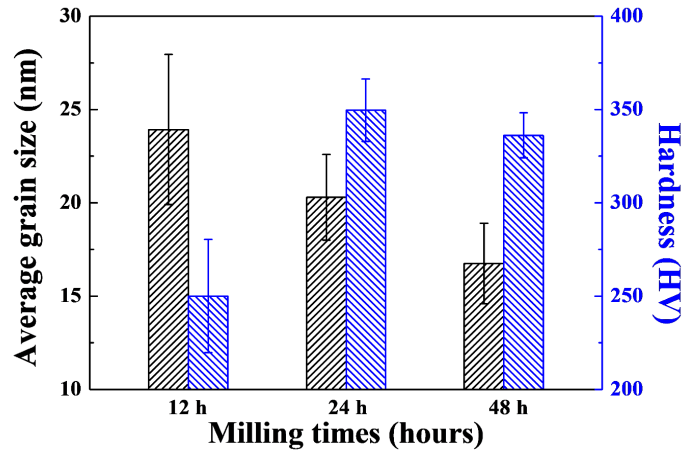
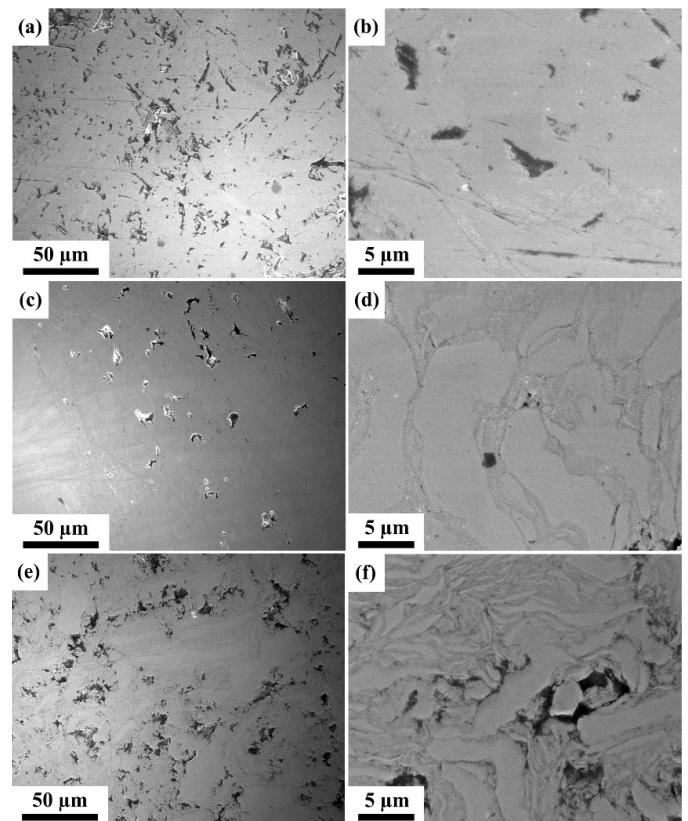


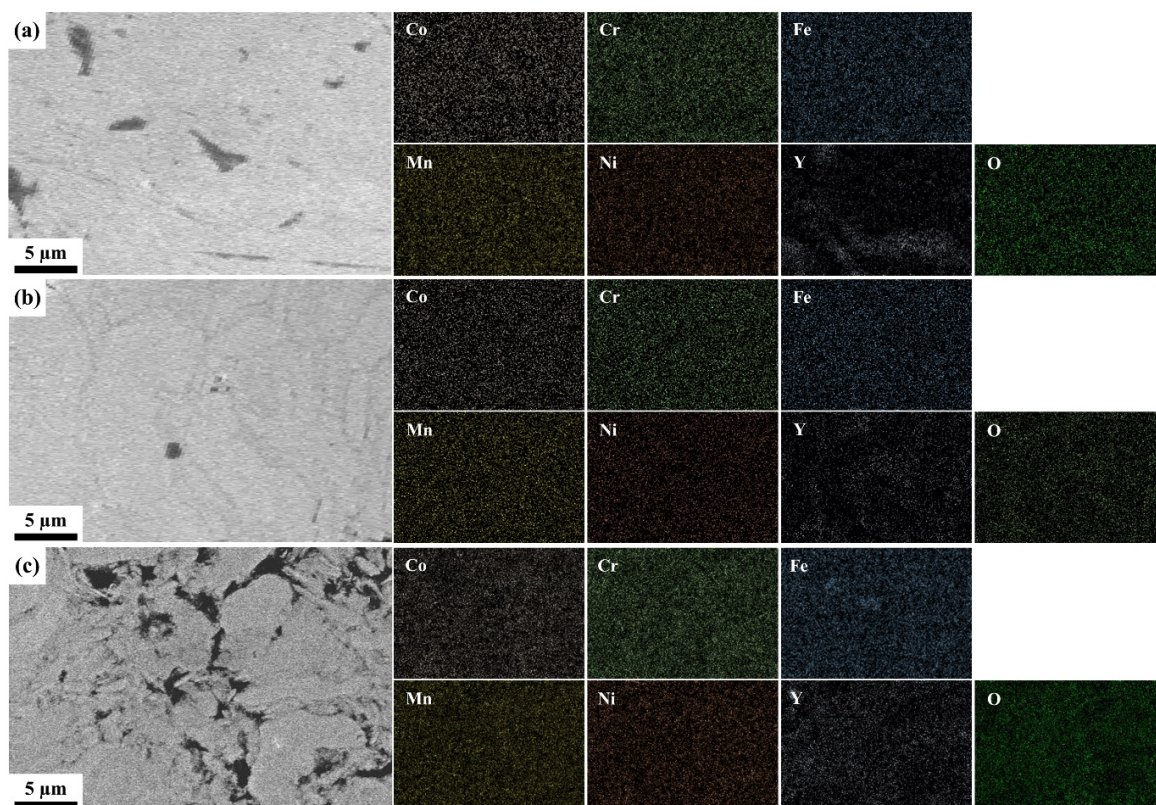
Fig. 5. Average grain size and Vickers hardness test results of the as-pressed composites under various milling durations (12, 24, and 48 h)

4. Conclusion

CoCrFeMnNi-based ODS composites were fabricated via high-energy ball milling with various milling times (12, 24, and 48 h) and hot-pressing processes. Longer milling times led to a reduction in the size of the HEA powder and Y_2O_3 particles. After hot pressing, grains were refined by severe plastic formation during the milling process. Moreover, the fraction of the in-situ phase within the composites increased with increasing milling time due to many crystalline defects. Unlike the other



Supplementary Fig. 2. Scanning-electron-microscope images of the as-pressed composites for various milling times: (a, b) 12 h, (c, d) 24 h, and (e, f) 48 h



Supplementary Fig. 3. Scanning-electron-microscope images and energy-dispersion spectroscopic maps of the as-pressed composites for various milling times: (a) 12 h, (b) 24 h, and (c) 48 h

composites, the 48-h-milled powder had only MnO_2 without MnO . This implies that the type of oxides in the composites is also influenced by the milling time. Optimal conditions led to fine grain size, high dispersion of Y_2O_3 nanoparticles, and the proper fraction of the in-situ second phase. The 24 h milling process was optimal; the corresponding as-pressed composite had the highest Vickers hardness (349.6 ± 16.73 HV).

REFERENCES

- [1] B. Cantor, I.T.H. Chang, P. Knight, A.J.B. Vincent, *Mater. Sci. Eng. A*. **375-377**, 213-218 (2004).
- [2] F. Otto, A. Dlouhý, Ch. Somsen, H. Bei, G. Eggeler, E.P. George, *Acta Mater.* **61**, 5743-5755 (2013).
- [3] G.T. Lee, J.W. Won, K.R. Lim, M. Kang, H.J. Kwon, Y.S. Na, Y.S. Choi, *Met. Mater. Int.* (2020).
DOI: <https://doi.org/10.1007/s12540-020-00786-7>
- [4] J.H. Kim, Y.S. Na, *Met. Mater. Int.* **25**, 296-303 (2019).
- [5] Y.Z. Tian, Y. Bai, M.C. Chen, A. Shibata, D. Terada, N. Tsuji, *Metall. Mater. Trans. A*, **45**, 5300-5304 (2014).
- [6] R. Zheng, T. Bhattacharjee, A. Shibata, T. Sasaki, K. Hono, M. Joshi, N. Tsuji, *Scr. Mater.* **131**, 1-5 (2017).
- [7] Y.Z. Tian, Y. Bai, L.J. Zhao, S. Gao, H.K. Yang, A. Shibata, Z.F. Zhang, N. Tsuji, *Mater. Charact.* **126**, 74-80 (2017).
- [8] A. Siahsarani, F. Samadpour, M.H. Mortazavi, G. Faraji, *Met. Mater. Int.* (2020).
DOI: <https://doi.org/10.1007/s12540-020-00828-0>
- [9] B. Schuh, F. Mendez-Martin, B. Völker, E.P. George, H. Clemens, R. Pippan, A. Hohenwarter, *Acta Mater.* **96**, 258-268 (2015).
- [10] H. Shahmir, J. He, Z. Lu, M. Kawasaki, T.G. Langdon, *Mater. Sci. Eng. A*. **676**, 294-303 (2016).
- [11] C.L. Chen, C.L. Huang, *Met. Mater. Int.* **19**, 1047-1051 (2013).
- [12] B. Gwalani, R.M. Pohan, O.A. Waseem, T. Alam, S.H. Hong, H.J. Ryu, R. Banerjee, *Scr. Mater.* **162**, 477-481 (2019).
- [13] L. Moravcik, L. Gouvea, V. Hornik, Z. Kovacova, M. Kitzmantel, E. Neubauer, I. Dlouhy, *Scr. Mater.* **157**, 24-29 (2018).
- [14] P. He, J. Hoffmann, A. Möslang, *J. Nucl. Mater.* **501**, 381-387 (2018).
- [15] J.M. Byun, S.W. Park, Y.D. Kim, *Met. Mater. Int.* **24**, 1309-1314 (2018).
- [16] A. Patra, S.K. Karak, S. Pal, *IOP Conf. Ser. Mater. Sci. Eng.* **75** (012032), 1-6 (2015).
- [17] S. Nam, S.E. Shin, J.H. Kim, H. Choi, *Met. Mater. Int.* **26**, 1385-1393 (2020).
- [18] N. Salah, S.S. Habib, Z.H. Khan, A. Memic, A. Azam, E. Alarfaj, N. Zahed, S. Al-Hamedi, *Int. J. Nanomed.* **6**, 863-869 (2011).
- [19] H. Shahmir, J. He, Z. Lu, M. Kawasaki, T.G. Langdon, *Mater. Sci. Eng. A*. **676**, 294-303 (2016).
- [20] N. Park, B.-J. Lee, N. Tsuji, *J. Alloys Compd.* **719**, 189-193 (2017).
- [21] Q. Wang, Z. Li, S. Pang, X. Li, C. Dong, P. Liaw, *Entropy* **20**, 878 (2018).
- [22] V. Rajkovic, D. Božić, A. Devečerski, *J. Serb. Che. Soc.* **72**, 45-53 (2007).
- [23] S.K. Vajpai, R.K. Dube, P. Chatterjee, S. Sangal, *Metall. Mater. Trans. A*. **43**, 2484-2499 (2012).